R. Mewe

High-resolution X-ray spectroscopy in astrophysics

ABSTRACT

The detection of X-rays from astrophysical sources has provided evidence for the existence of a large variety of stellar, interstellar and extragalactic plasmas with temperatures above one million Kelvin. High-resolution X-ray spectroscopy of such plasmas will allow a detailed study of the physical processes that release the energy and maintain these plasmas. In particular the spectroscopic space missions near the end of the century, viz. NASA's Advanced X-ray Astrophysics Facility (*AXAF*) and ESA's X-ray Multi-Mirror Mission (*XMM*) give astronomers the opportunity to measure many emission and absorption features with a resolution of $\sim$ 0.05 Å in the wavelength range $\sim$ 1–300 Å, allowing them to interpret much better the origins of the different spectral components. To illustrate the diagnostic capabilities of such observations spectral simulations are shown for various types of cosmic sources.

1. INTRODUCTION

Traditionally X-ray spectroscopic results in astrophysics were obtained with instruments used for photometry, viz. proportional counters which have only a limited resolving power, allowing merely to determine the overall shape of the spectrum. Typically, one characterized the X-ray spectrum of a cosmic source by indicating whether it was best fit by simple blackbody, thermal bremsstrahlung, or power law models. In recent years, the introduction of solid state and transmission grating spectrometers on the *EINSTEIN* and *EXOSAT* satellites with somewhat higher spectral resolution (e.g. $\lambda/\Delta\lambda$ = 10–100) has provided a taste of detailed spectroscopy of cosmic plasmas and motivated the use of more sophisticated emission models, which include the line emission expected from hot optically thin plasmas in collisional ionization equilibrium (e.g. Raymond and Smith 1977, Mewe *et al.* 1985, 1986). However, since most of the lines are not explicitly spectrally resolved, the spectral constraints derived are still highly model-dependent.

High-resolution spectroscopy in the soft X-ray wavelength region ($\sim$ 2–140 Å) such as will be possible with the next generation of spectroscopic X-ray satellites *AXAF* (Weisskopf 1987) and *XMM* (Barr *et al.* 1988) will allow astronomers to individually detect and identify many of the expected discrete soft X-ray spectral features for many different classes of cosmic sources.

Some of the spectrometers that are currently foreseen on these missions are: the High-Energy Transmission Grating (*HETG*) on *AXAF* (Canizares *et al.* 1987) (with a spectral range $\lambda\lambda \simeq$ 2–30 Å, a spectral resolution $\Delta\lambda \sim$ 0.02 Å, and an effective area A of up to $\sim$ 200 cm^2 between 4–10 Å), the Low-Energy Transmission Grating Spectrometer (*LETGS*) on *AXAF* (Brinkman *et al.* 1987) ($\lambda\lambda \simeq$ 4–140 Å, $\Delta\lambda \simeq$ 0.05 Å, and A up to $\sim$ 30 cm^2 between 6–50 Å), and the Reflection Grating Spectrometer (*RGS*) on *XMM* ($\lambda\lambda \simeq$ 5–35 Å, $\Delta\lambda \simeq$ 0.05 Å, and A up to $\sim$ 250 cm^2 between 10–20 Å).

Contained in the above wavelength regions are a multitude of prominent features from nearly all ion stages of many abundant elements, including the K-shell line and continuum transitions of C, N, O, Ne, Mg, and Si, and the L-shell transitions of Si, S, Ar, Ca, Ni, and Fe. Many of these features will be detected either in emission or absorption for a large variety of different astrophysical plasmas including: stellar coronae, isolated hot white dwarfs, cataclysmic variables, X-ray binaries, supernova remnants, the interstellar medium, normal galaxies, clusters of galaxies, and active galactic nuclei. The detection of emission and absorption features allows to uniquely determine the most important physical parameters for these plasmas including the electron temperature and density distributions, the ion and elemental abundances, mass motions, and the nature of the ambient radiation field. The spectroscopic data we expect to obtain will provide the most direct insight into the physical phenomena that drive the X-ray energy release and will likely provide an enormously important new tool for the study of virtually all known cosmic X-ray sources. Thus high-resolution X-ray spectroscopy represents one of the final observational frontiers for high-energy astrophysics.

In the following sections I briefly discuss the physics determining the formation of X-ray spectra in various types of plasmas, present a few observational results and focus specifically on a number of simulations of spectral observations with the *AXAF* and *XMM* spectrometers for various types of cosmic sources.

2. SPECTRA FORMATION IN PLASMAS

The spectral properties of the emitted radiation will greatly vary with the different physical conditions of spectral line formation in various kinds of astrophysical plasmas. Rather than attempt to include all we know about the physics of X-ray sources, I consider a limited number of highly simplified models (once we have gained a better understanding of the source structure and of the importance of various physical processes, we may synthesize such models into successively more sophisticated approximations of the source model). I distinguish between three categories of plasma models applicable to the cosmic sources which are expected to exhibit soft X-ray spectra (for reviews see e.g. Holt and McCray 1982, McCray 1982, 1984, Mewe 1984, Barr *et al.* 1988): optically thin plasmas, nebular-type photo-ionized plasmas, and optically thick plasmas.

2.1. *Optically thin thermal plasmas*

In a hot optically thin plasma that is sufficiently transparent that the transfer of radiation can be neglected the emergent X-ray spectrum faithfully represents the microscopic emission processes in the plasma and therefore is directly linked to the physical conditions in the plasma. This is the standard *coronal model* that was first applied by Elwert (1952) to the solar corona. It assumes a tenuous plasma in a steady state in which electron collisions control the ionization state and emissivity of the gas. The gas is in a state of statistical equilibrium both for the bound atomic states and for the ionization balance and the plasma electrons and the ions are relaxed to Maxwellian energy distributions with a common temperature, T, a free parameter controlled by external processes. Examples of such plasmas are stellar coronae, supernova remnants, and the hot gas in the interstellar medium and in galaxies and clusters, and possibly also the low-density intercloud medium that pervades most of the central broad-line region in active galactic nuclei.

2.1.1. Ionization state. Much of the temperature sensitivity of the soft X-ray spectrum is associated with the ionization structure which is determined by a balance between electron impact ionization (including sometimes a contribution from autoionization) and radiative plus dielectronic recombination.

As an example Figure 1 shows the iron ionization structure as a function of temperature as calculated by different authors (Arnaud and Rothenflug (1985) (AR) and Raymond and Smith (1977), Raymond (1988) (RS)). As can be seen, it varies dramatically with temperature throughout the range 0.1–100 MK. On the basis of the estimated uncertainties (20–40%) in both ionization and recombination rates (for a discussion see e.g. Raymond 1988, 1989, Mewe 1989), we can expect the predicted ratio of ion concentrations of adjacent ionization stages to be off by a factor, say ~1.5–2. Fortunately, the ionization and recombination rates for the H- and He-like ions, which emit the lines that are among the strongest from hot astrophysical plasmas, are known more accurately than most of the other rates. In the case of ions which have a closed outer electron shell (e.g. He- and Ne-like ions) it doesn't matter very much because such ions cover a broad plateau in dependence of temperature (see Figure 1). This is caused by the fact that this ionization stage can easily be reached from the Li-like stage (only one outer electron with low binding energy) and persists long since the next ionization step towards the H-like stage suddenly needs a much (~4 times) higher ionization energy. This implies that the adjacent Li-like stage is quite critically dependent on temperature. But such ions can still exist when the plasma is not isothermal, but instead has a broad distribution of temperatures (as is often the case, e.g. in stellar coronae or in supernova remnants).

Comparing the AR and RS results, we notice that the overall shapes of the curves are quite similar and that the shifts of the ion peaks are generally limited to within about $\Delta \log T \approx 0.1$. However, the peak values may differ by about 10–30% and sometimes up to ~ 50%. The differences often result from different dielectronic recombination rates (cf. Raymond 1988). The discrepancies are worst for the lower stages of ionization (e.g. Fe VIII and Fe IX), but nearly vanish for the simpler and more thoroughly studied ions of the He- and H-like sequences. Generally, the discrepancy is ~ 10–20% in T, which for many diagnostic purposes is good enough. On the other hand, for a given temperature, the ion abundances may differ by a factor up to about two, especially for the ions just around the He-like and Ne-like "plateaus". For diagnostics of tenuous plasmas the AR ionization balance computations can be used with reasonable accuracy.

However, a few words may be said about possible effects of electric fields on dielectronic recombination (DR) rates. Experimental breakthroughs occurred about five years ago when DR cross sections could be measured for a few singly ionized atoms (e.g. Mg^+ and Ca^+) in crossed-beam experiments (e.g. Hahn 1985, Müller *et al.* 1987 and Dunn 1986). The measured cross-section values were a factor ~ 5–10 larger than predicted ones. A possible explanation of this strong discrepancy was given in terms of the effect of an electric field that causes Stark mixing of different ℓ levels of a given n state. In the experiment, a magnetic field $B \sim 200$ Gauss was used to focus the electron beam. The ions which cross the electron beam with velocities $v \sim 10^7$ cm/s then experience in their rest frame a Lorentz field $E = 10^{-8} vB \approx 20$V/cm, sufficient to produce full Stark mixing. The explanation is as follows. As A_a decreases rapidly with ℓ and as DR rates scale $\propto A_a A_r/(A_a + A_r)$ (A_a, A_r are probabilities for autoionization and radiative decay, resp.) the contribution of resonant states is limited to $\ell \lesssim \ell_c$ (for which $A_a \gtrsim A_r$). The result of mixing high and low ℓ levels is that A_a is increased for high ℓ and decreased for low ℓ, thus flattening the $A_a(\ell)$ versus ℓ curve, so that more states effectively participate in the recombination process, and the DR cross section is increased. In the actual plasma environment the mean thermal drift of ions across a magnetic field of a few hundred Gauss may well generate such Lorentz electric fields (e.g. in solar or stellar coronal loop structures).

Though the effects of electric fields are yet to be fully incorporated into future DR rate calculations, it is interesting to visualize this effect on the hand of a simple model (see Müller *et al.* 1987). The typical enhancement factor for the DR recombination of ion $Z^{+(z+1)}$ due to full Stark mixing I approximate by $f = 1 + 10\,(z+1)^{-1.15}$. (We note that the effects are biggest for the lower ions as here many n states take part in the DR process). Figure 2 compares the results for the AR oxygen and iron ionization balance without and with correction for the DR rates. This illustrates that this effect can be important for the lowly ionized atoms that are formed e.g. in cool ($\lesssim$ 2 MK) coronal or photoionized plasmas.

2.1.2. Line excitation and spectra. The spectral lines that dominate the soft X-ray spectrum and the cooling of astrophysical plasmas at temperatures up to ~ 10 MK are mainly excited by electron collisional excitation from the ground state, followed by spontaneous radiative decay from the upper line level. The formation of a particular spectral line transition $2 \rightarrow 1$ emitted by ion Z^{+z} from element of atomic number Z is as follows. The total depopulation rate of the upper level (2) is equal to $N_2 \sum_i A_{2i}$, where N_2 is the density (cm^{-3}) of ions in the upper level 2 and A_{2i} is the probability (s^{-1}) of a spontaneous radiative transition from level 2 towards a lower level i (collisional de-excitation is neglected here). This will be balanced by electron collisional excitations from the ground state (g) at a rate $n_e N_g S_{g2}$, so that the volume emissivity P_{21} (phot cm^{-3} s^{-1}) is given by

$$P_{21} = N_2 A_{21} = n_e N_g B S(T) = (N_H/n_e) A_Z n_e^2 \eta_z B S(T), \quad (1)$$

where n_e is the plasma electron density (cm^{-3}), $S(T)$ is the rate coefficient ($cm^3\ s^{-1}$) for collisional excitation $g \rightarrow 2$ (dependent on electron temperature T), $B = A_{21}/\sum_i A_{2i}$ is the radiative branching ratio, N_g the ground state population (cm^{-3}) of ion Z^{+z}, $A_Z = N_Z/N_H$ the abundance of element Z relative to hydrogen (H), η_z the fraction of ions from element Z in ionization stage z and N_H/n_e is of the order unity ($\simeq$ 0.85) for a plasma with cosmic abundances. The excitation rate coefficient can be written as:

$$S(T) = 8.62\ 10^{-6}\ \frac{\bar{\Omega}(y)}{\omega T_{[K]}^{1/2}} \exp(-y)\ (cm^3\ s^{-1}), \quad (2)$$

where $y = E_0/kT$, E_0 is the excitation threshold energy, ω is the statistical weight of the initial (usually ground) level and $\bar{\Omega}(y)$ is the collision strength averaged over the Maxwellian electron energy distribution. Some time ago I have introduced (e.g. Mewe 1972, Mewe and Schrijver 1978, Mewe 1988) a parametrized interpolation formula for Ω that represents the correct behaviour near threshold and asymptotically at high energies and that can be integrated analytically over the Maxwellian electron energy distribution. We have used such an expression to fit to many available theoretical and experimental data for excitation cross sections or rates. When no data are available one can make use, for a rough estimate, in the case of optically allowed dipole transitions, of the Gaunt factor formula:

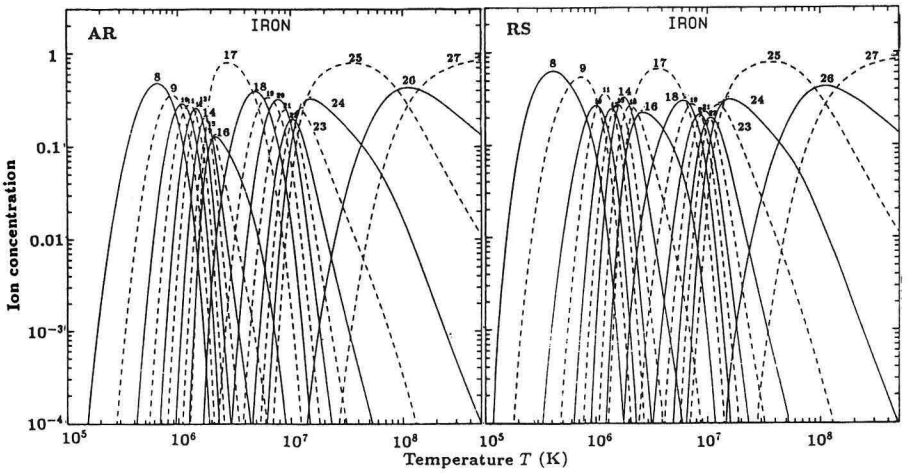

Fig. 1. Ion fractions as a function of temperature for iron as calculated by AR and RS (see text). Ion stages are designated by numbers, e.g. 8 indicates ion Z^{+7} (Fe VIII), etc.

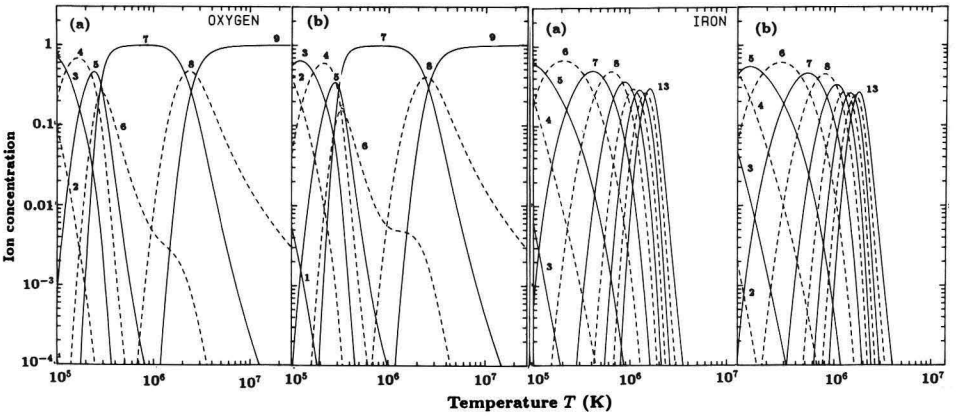

Fig. 2. Ion fractions for O and Fe as calculated for the AR ionization balance without (a) and with (b) correction for ℓ level Stark mixing.

$$\bar{\Omega} = \frac{8\pi}{\sqrt{3}} \frac{E_H}{E_0} \omega f \bar{g} = 197.3\, \omega f \bar{g} E_{0[\mathrm{eV}]}^{-1}, \qquad (3)$$

where f is the absorption oscillator strength and $\bar{g} \equiv \bar{g}(y)$ the average Gaunt factor. With an accuracy of a factor of two or so typically $\bar{g} \sim 0.2$ for $\Delta n \neq 0$ transitions and ~ 1 for $\Delta n = 0$ transitions.

Though in a number of cases the Gaunt factor approximation method gives reasonably accurate results, more accurate values are needed, especially for the weaker lines and optically forbidden transitions. Raymond (1988) gives a brief discussion of the accuracy of several computational methods such as Coulomb-Born (CB) and Distorted Wave (DW) approximations, and the more accurate Close Coupling (CC) method, which properly takes into account the dominant resonances near the threshold of excitation (for a review of theory see Seaton (1975), of crossed-beam experiments see Dolder and Peart (1986), and of plasma measurements of atomic rates see Griem (1988)). CB tends to overestimate the collision strength near threshold by $\sim$ 20–50%, while DW gives better results, especially for high-Z ions. Few accurate CC results are available for He-like ions (Kingston and Tayal 1983). Recent compilations of excitation collision strengths are reported by Aggarwal *et al.* (1985) and by Gallagher and Pradhan (1985). For many of the strongest X-ray lines, e.g. from H- and He-like ions and Li- to Ne-like ions, the collision strengths are known with better than 20% accuracy. Near threshold, the strong resonances may spoil the accuracy. However, for applications of rate coefficients in plasma diagnostics, we should not worry too much about this, because in averaging the cross section over the electron energy distribution we smooth out these resonances for a great deal.

Furthermore, there is an additional contribution to the X-ray spectrum from continuum emission due to bremsstrahlung, recombination, and two-photon emission from H- and He-like ions (Mewe *et al.* 1986).

The overall appearance of the X-ray spectra will be dominated by the ionization structure. Therefore, in a wide temperature range (0.01–10 MK) the X-ray spectra of optically thin sources are rich in emission lines from many ions of a number of cosmically abundant elements in different ionization stages. In extremely hot ($\gtrsim$ 100 MK) plasmas all abundant elements are nearly fully ionized and the X-ray emission is dominated by continuum radiation. The emission line and continuum X-ray spectra have been reasonably accurately calculated (e.g. Raymond and Smith 1977, Mewe *et al.* 1985, 1986). From a comparison between different calculations Raymond (1988) concludes that for the strongest X-ray lines, e.g. those of the H- and He-like ions, the agreement generally approaches about 20% (which is important because the He-like lines can be used for density diagnostics), whereas for other cases (e.g. iron lines around 10–12 Å and silicon and sulphur lines around 40–50 Å) discrepancies of a factor of two may exist due to the uncertainties in the atomic rates for excitation

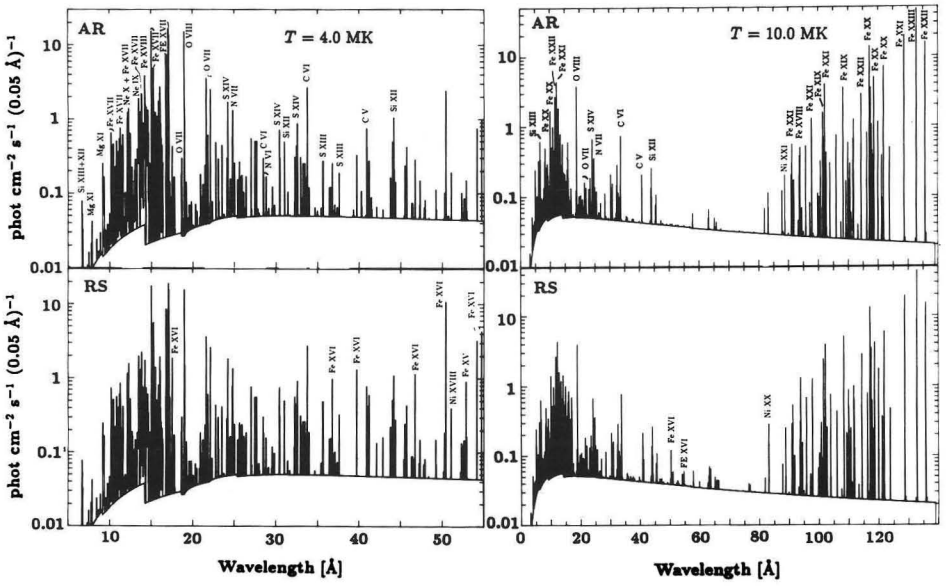

Fig. 3. Comparison of various optically thin X-ray spectra calculated for different ionization balances (AR: Arnaud and Rothenflug, RS: Raymond and Smith) for temperature T = 4 MK and 10 MK, reduced emission measure ε/d^2=10^{50} cm^{-3} pc^{-2} (d is source distance), and wavelength regions 5–55 Å and 3–140 Å, respectively. The intrinsic spectral lines are assumed to be Doppler-broadened corresponding to the temperature T. The most prominent lines are labelled with the corresponding ion species. The spectra are binned in 0.05 Å intervals. The most prominent lines are labelled with the corresponding ion species. The contribution from the continuum radiation is separately indicated by a solid line. In all calculations excitation rates from Mewe *et al.* (1985) are used.

and ionization. A comparison in Figure 3 of theoretical spectra derived using two different ionization balance calculations (AR vs. RS) for isothermal, cosmic abundance plasmas at $T = 4$ and 10 MK, respectively, confirms the above conclusions. Figure 3 also illustrates that the X-ray spectrum is very sensitive to the electron temperature, so that a measurement of the spectrum provides an extremely sensitive temperature diagnostic. Substantial differences are observed for the two cases, not only in the overall shape of the spectral energy distribution, but also in the detailed line structure in virtually every narrow wavelength band. In some cases the line strengths are sensitive to the electron density and in certain circumstances also to deviations from the ionization equilibrium (e.g. transient plasmas in supernova remnants or solar flares) or to deviations from Maxwellian electron energy distributions (e.g. solar flares).

2.1.3. Differential emission measure modelling. Eq. (1) shows that for an optically thin isothermal plasma with cosmic abundances the line intensity integrated over the whole source volume V (cm^3) is proportional to the well-known total *emission measure* $\varepsilon \equiv \int n_e^2 dV$ (cm^{-3}) of the source, but for a general (and more realistic) multi-temperature structure in the plasma the situation is more complicated. In this case we can make use in the analysis of optically thin spectra of the concept of a differential emission measure (DEM) distribution, which is defined as follows. For a multi-temperature plasma the line strength can be expressed as $\propto \int S(T) n_e^2 dV \equiv \int S(T)\varphi(T)dT$, where $\varphi(T) = n_e^2 \frac{dV}{dT}$ (cm^{-3} K^{-1}) is the so called *differential emission measure* (which also can be used to describe the continuum emission). Note that the total emission measure is given by $\varepsilon = \int n_e^2 dV = \int \varphi(T) dT$. The differential emission measure distribution can be derived from the observed spectrum by deconvolving $\varphi(T)$ from the measured spectral intensities, using known emission functions for the individual wavelength bins. For this deconvolution we can apply an iterative technique which uses an initial form for the differential emission measure, $\varphi_0(T)$, to calculate theoretical line intensities, i.e. the Withbroe-Sylwester iteration scheme based on a method proposed by Withbroe (1975) and modified by Sylwester *et al.* (1980). Lemen *et al.* (1989) have applied this technique to analyze the *EXOSAT* X-ray spectra of stellar coronae, but this method can be applied equally well to investigate the temperature structures of other kinds of optically thin plasmas such as supernova remnants and cooling flows in clusters of galaxies.

2.1.4. Electron density diagnostics. Determination of electron densities n_e in hot cosmic plasmas provides another challenge for X-ray astronomy. In combination with a determination of the emission measure $\varepsilon = \int n_e^2 dV$ from spectral fits a value derived for the electron density will provide direct information about the emitting source volume V. In order to test current theoretical models of the X-ray source, it is very important to establish its size. Electron densities can be measured using density-sensitive spectral lines originating from metastable levels or using innershell excitation satellites to resonance lines (e.g. Mewe 1988). In the first case the He-like $2 \rightarrow 1$ triplet system lines are particularly important (Gabriel and Jordan 1969, Pradhan and Shull 1981, Pradhan 1982, 1985, Mewe *et al.* 1985). The intensity ratio of the forbidden (f) to intercombination (i) lines varies with electron density due to the collisional coupling between the metastable 2^3S upper level of the forbidden line and the 2^3P upper level of the intercombination line. The f/i line intensity ratio in the wavelength region 5–42 Å of He-like ions from C through S can be used to diagnose coronal plasmas in the density range $n_e = 10^8$–10^{15} cm^{-3} and corresponding temperature range $T \sim$ 1–20 MK. Figure 4 shows the expected O VII line strengths with 0.05 Å resolution, for a coronal plasma with a temperature of 2 MK and densities of 10^{10}, 10^{11}, and 10^{12} cm^{-3}, respectively.

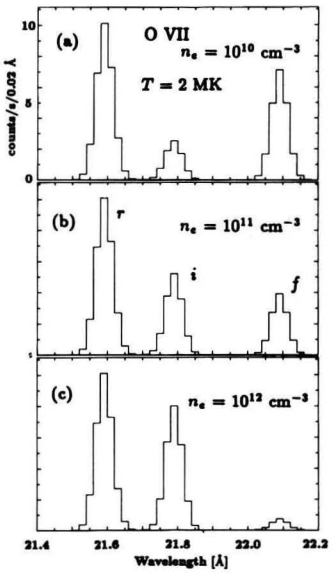

Fig. 4. O VII triplet at 22 Å as observed with the *XMM-RGS* for $T = 2$ MK, $n_e = 10^{10}$, 10^{11} and 10^{12} cm^{-3} and $\varepsilon/d^2 = 10^{52}$ cm^{-3} pc^{-2}. Symbols r,i,f indicate the resonance, intercombination, and forbidden line, respectively.

2.1.5. Deviations from the coronal approximation. Apart from the uncertainties of the basic atomic parameters (typically $\sim$ 30–50%), other uncertainties can arise from the simplifying assumptions made in the coronal model. Raymond (1988) and Mewe (1989) have discussed several effects of relaxing the restrictions by considering optical depth and high-density effects, and deviations from a Maxwell distribution or from ionization equilibrium in transient plasmas.

2.1.6. Examples of spectra from optically thin sources. Because the emission line spectra and continua from optically thin plasmas are fairly well known, high-resolution X-ray spectroscopy has its most obvious application in the measurement of optically thin sources such as the *coronae of stars*. X-ray observations with the *EINSTEIN* observatory have demonstrated that soft X-ray emitting coronae are a common feature among stars on the cool side of the Hertzsprung-Russell diagram. Observations with the transmission grating spectrometers (*TGS*) aboard *EINSTEIN* (Mewe *et al.* 1982) and *EXOSAT* (Schrijver 1985, Lemen *et al.* 1989, Schrijver *et al.* 1989) and with the solid state spectrometer (*SSS*) on *EINSTEIN* (Swank *et al.* 1981) have shown that data of even modest spectral resolution

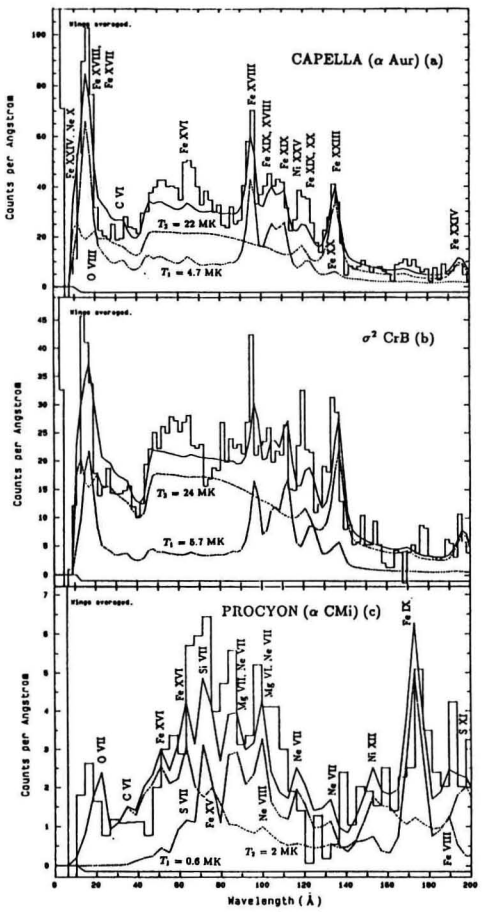

Fig. 5. *EXOSAT* 500 lines/mm *TGS* spectra of Capella (a), σ^2 CrB (b) (binned in 2 Å bins), and Procyon (c) (binned in 4 Å bins), compared with the best-fit two-temperature spectrum (continuous line). The two temperature components 1 and 2 are shown separately by a dotted or a dash-dotted line, respectively. The most prominent lines are labelled with the corresponding ion species.

($\lambda/\Delta\lambda$= 10-100) allows the identification of coronal material at different temperatures whose existence may relate to a range of possible magnetic loop structures in the outer atmospheres of these stars. Comparison of measured line fluxes with known theoretical emissivities yields the DEM distribution with temperature, which is an essential first step in building a model for a stellar corona and assessing the important terms in the coronal energy balance. Figure 5 shows the results obtained with the *EXOSAT-TGS* with $\sim$ 3 Å resolution for three different late-type stars. Some interesting points readily emerge from an identification of the spectral lines and line complexes in these spectra. The active stars Capella and σ^2 CrB show a prominent Fe XXIII line at 133 Å which is typical for hot plasmas with temperatures T of about 10–20 MK, such as observed in solar flares (e.g. Mason *et al.* 1984). This line is absent in the spectrum of the much cooler corona ($T \simeq 0.6$ MK) of the star Procyon, which contains instead a strong blend of lines around 170 Å, that can be identified as a group of spectral lines from Fe IX–XI ions (formed at T in the range 0.6–2 MK). On the other hand, this 170 Å emission feature is not present in the spectra of Capella and σ^2 CrB which implies that only relatively little plasma cooler than 2 MK can be present in the coronae of these stars. This conclusion is supported by the narrowness of the Fe XVII–XVIII line complex at 15 Å: if much plasma with temperatures below 2 MK were present, this complex would be broadened by O VII lines at 21.6 Å and 22.1 Å. The intensity ratio of the 15 Å Fe XVII-XVIII line complex and the Fe XVIII–XXIII line complex between 90–140 Å demonstrates that the spectra cannot be emitted by an isothermal plasma, but instead requires at least a two-temperature interpretation. On the basis of a detailed DEM analysis Lemen *et al.* (1989) confirm that the emission of the corona of each of these stars is dominated by plasma in two relatively narrow temperature intervals: 5 MK and 25 MK for Capella and σ^2 CrB, and 0.6 MK and $\sim$ 2 MK for Procyon. By analogy with the Sun, the outer atmospheres of cool stars with a convection zone are generally assumed to consist of magnetic loop structures filled with hot plasma, which connect opposite polarities in the photosphere. The DEM distributions as provided by such loop models suggest model coronae comprising two distinct ensembles of quasi-static magnetic loops with maximum temperatures around the dominant temperatures given above (Schrijver *et al.* 1989).

The improved spectral resolution of the next generation of spectrometers aboard *XMM* and *AXAF* is needed to fully resolve the temperature structure of stellar coronae, as is shown in Figure 6 which compares between simulations for transmission grating spectra from *AXAF* and *EXOSAT*.

Another important class of thin X-ray sources are the *remnants of supernova explosions*, which play a dominant role in the heating and the replenishment (hence the enrichment by heavy elements) of matter in the surrounding interstellar medium. Supernova explosions, dramatic events in themselves, have also profound and long lasting effects on the appearance and future evolution of the galaxies in which they occur. Following a stellar explosion a substantial fraction of the star's mass is ejected at high velocity into the surrounding interstellar medium and the visible manifestations of such an event are collectively described by the term supernova remnant (SNR). For young remnants (i.e. those with age $\lesssim 10^4$ years) the associated high-temperature plasma is mostly comprised of ejected material, whereas for the old remnants the plasma results from the ambient interstellar gas that has been heated by the passage of the shock wave from the explosion. In either case, plasma temperatures are in the range above 1 MK and hence observations of spectrally resolved X-ray emission lines provide the most useful information about this hot gas.

The detection and analysis of the X-ray emission spectra of recently detected extragalactic supernovae will be of particular importance. The recent observation of hard X-rays from the supernova SN1987A raises the very interesting possibility

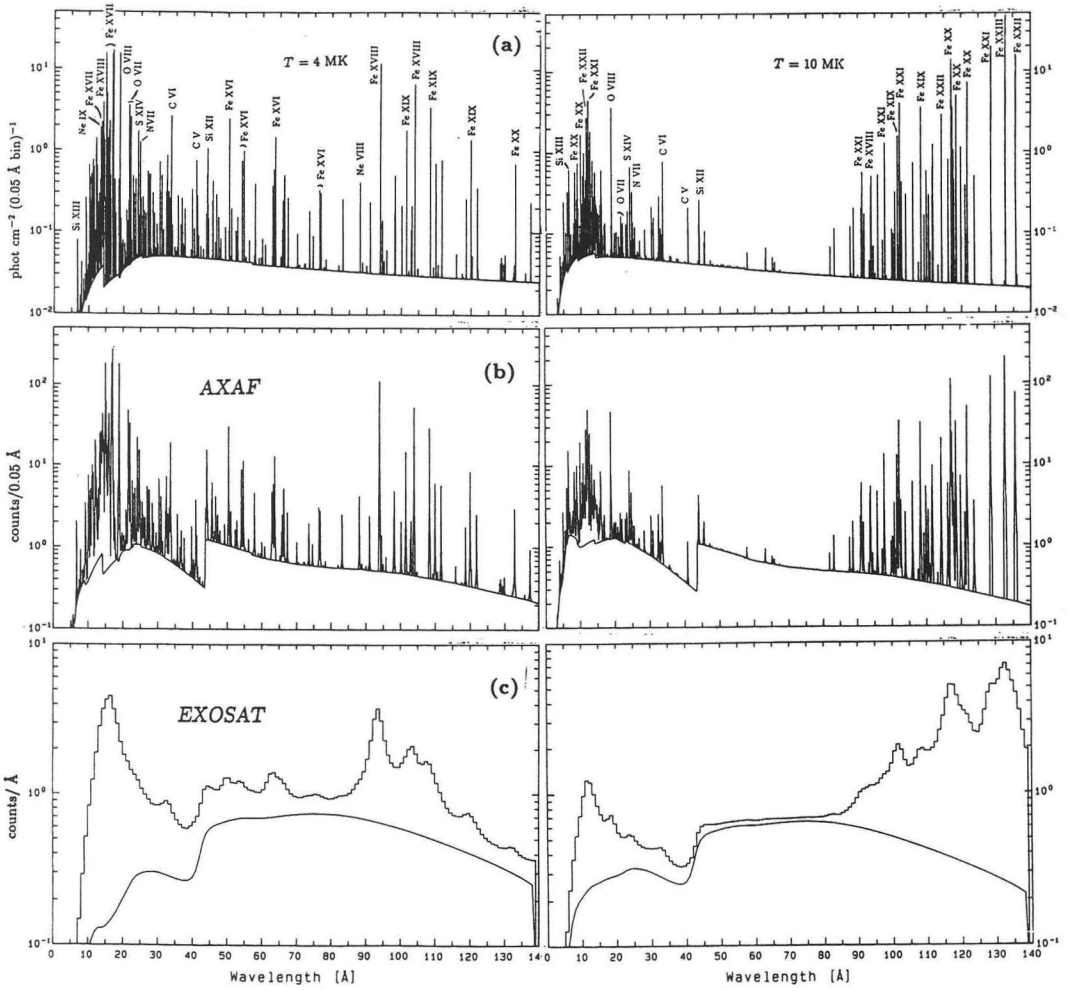

Fig. 6. Panel a: incident photon flux spectra between 3–140 Å, integrated over 10^4 s, calculated for an optically thin plasma with temperature $T = 4$ and 10 MK, reduced emission measure $\epsilon/d^2 = 10^{50}$ cm^{-3} pc^{-2}. The most prominent lines are labelled with the corresponding ion species. Panels b and c: Incident spectra convolved with the response of *AXAF-LETGS* and *EXOSAT-TGS*, respectively. The upper curves in panels c are the total line plus continuum spectra, whereas the bottom curves represent the contribution from the continuum radiation only.

of detecting soft X-rays from the remnant during the lifetime of *XMM*. An indication of the power of future X-ray spectroscopy for these studies is provided by Figure 7 which exhibits a simulation of a two-component spectrum of a Puppis A type SNR placed at a distance of 55 kpc in the Large Magellanic Cloud.

Finally, I consider the *clusters of galaxies* which are prominent X-ray sources due to the presence of hot intracluster gas. The discovery of iron line emission at $\sim$ 6.7 keV has demonstrated that such intracluster gas must have been processed in stars within the galaxies, since it is enriched with heavy elements. An accurate determination of the temperature of this gas (10-100 MK) provides the opportunity to measure the gravitational cluster potential, since the gas must be close to hydrostatic equilibrium. This gives an indication of the "hidden" mass in the cluster which appears to be a common constituent of our Universe. The gas density within the core of a cluster is generally so high that radiative cooling is important and an inflow of gas takes place onto the central galaxy. The mass flow of the cooling gas is estimated to reach sometimes very large values of up to 400 solar masses per year, which implies that the total accumulation of matter can be comparable to the mass ($10^{12} M_\odot$) of a whole large galaxy. The simple presence or

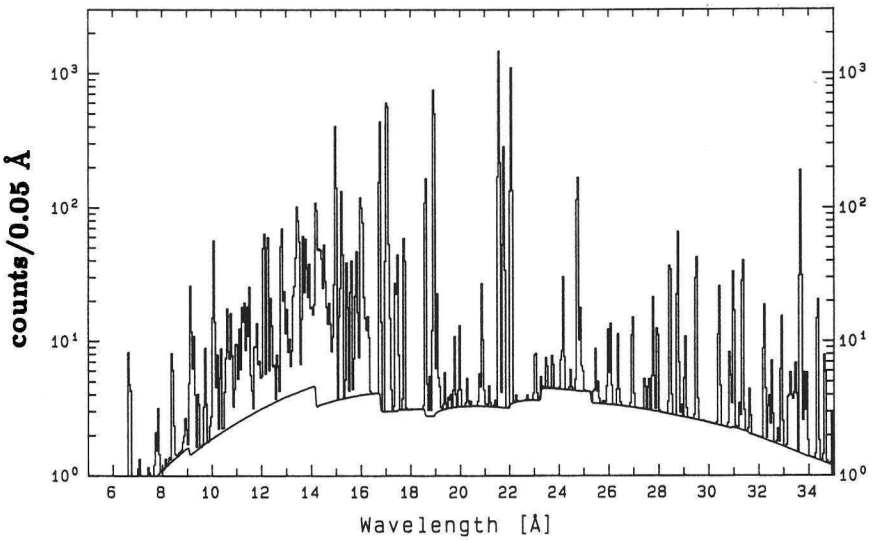

Fig. 7. A simulation of the spectrum of the Puppis A supernova remnant as seen through the *XMM-RGS* in 10^4 s for the case where the source is placed at the distance (55 kpc) of the Large Magellanic Cloud. At this distance, the finite source extent does not appreciably degrade the instrument spectral resolution. Assumed parameters: temperatures T_1=2 MK, T_2=7 MK, emission measures ε_1=1.8 10^{59} cm^{-3}, ε_2=4 10^{58} cm^{-3} and a correction for the interstellar absorption with a hydrogen column density N_H=5 10^{20} cm^{-2}.

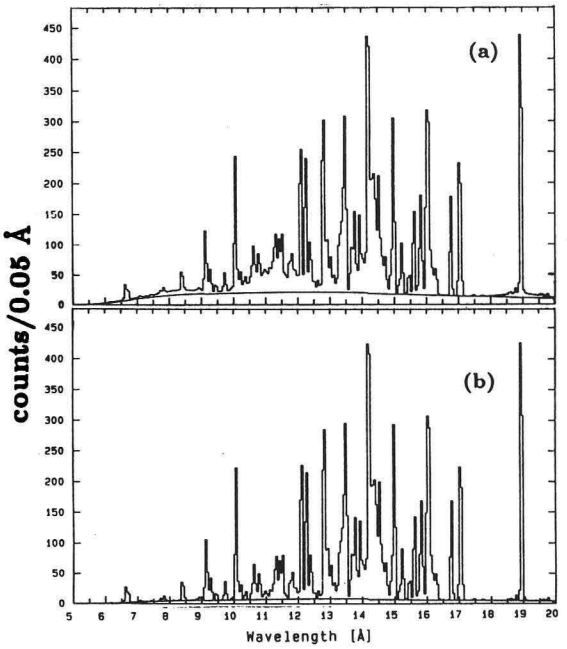

Fig. 8. Two-temperature spectrum of the cooling flow onto M87 in the Virgo cluster, folded through the response of the *XMM-RGS* for an observation time of 10^4 s. Top panel (a) shows the total spectrum of cooling flow (T_1=7 MK) and hot cluster gas (T_2=20 MK), bottom panel (b) shows the (dominant) contribution of the cooling flow only. Interstellar hydrogen column density $N_H = 10^{21}$ cm^{-2}. At the distance of 20 Mpc the cooling flow can be considered as a point source, but the finite extent of the hot gas component appreciably degrades the instrumental resolution and efficiency.

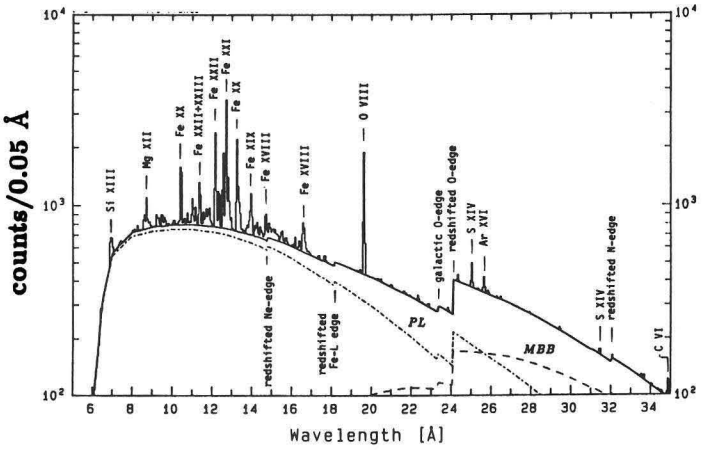

Fig. 9. Typical AGN spectrum as observed with the *XMM-RGS* in 10^5 s. The contributions from power law (PL) and modified black body (MBB) spectra are separately plotted (for details see text). O I absorption edge from our galaxy and various redshifted absorption edges and prominent emission lines from the source are indicated.

absence of certain spectral lines defines the temperature distribution in the source. Figure 8 shows the simulated *XMM-RGS* spectrum of the cooling flow onto the massive galaxy M87 at the core of the Virgo cluster. A simple two-temperature model has been used (parameters from Lea *et al.* (1982)). With a relatively short (10^4 s) exposure the emission lines of the cooling flow are bright and well resolved, whereas the lines from the hot component are smeared out due to the finite source extent and give only a minor contribution.

The most efficient energy sources known occur in *active galactic nuclei* (AGN). It is generally considered that accretion onto a supermassive black hole is the basic underlying process, which can be more than an order of magnitude more efficient in converting restmass to energy than is nuclear fusion. Detailed X-ray spectral studies are essential in understanding the accretion of matter onto such huge compact objects. Clearly this is of primary importance for testing the laws of physics under extreme conditions.

Current models of the X-ray emission of AGN distinguish between a hard X-ray power-law component and a soft excess above $\sim$ 25 Å. The hard component is usually attributed to non-thermal radiation from the central source that is inverse Compton scattered by very energetic electrons. The soft component is associated with the hotter parts of the accretion disk and described by a modified blackbody spectrum or it may be thermal bremsstrahlung of tenuous gas, in both cases with temperatures in the range 0.3–1 MK. Hence the absence or presence of spectral lines will show the true nature of this soft X-ray excess.

In some AGN there is evidence for another soft component of which the origin is presently unknown. Optical measurements show that the central region (radius $\sim$ 0.3 pc) contains dense ($\sim 10^9$ cm^{-3}) blobs of cool ($\sim$ 0.01 MK) gas with velocities $\sim 10^4$ km/s, the so called broad line region (BLR). It may be possible that the soft X-rays are emitted by a hot ($\sim$ 10 MK) tenuous ($\sim 10^6$ cm^{-3}) and *optically thin* gas that is in pressure equilibrium with these clouds and that pervades most of this central volume. High-resolution X-ray spectroscopy with the possibility to detect lines will be the ultimate tool to probe the physical conditions in the cores of AGN. To illustrate this I show in Figure 9 an example of a typical AGN spectrum folded through the *XMM-RGS* response (Kaastra *et al.* 1989). Three components are included: a power law with photon index -1.7 (average parameters from 3C 120, cf. Petre *et al.* (1984)), thermal line and bremsstrahlung with temperature 10 MK and emission measure 2 10^{66} cm^{-3} (parameters from 3C 120) and modified blackbody emission with temperature 1 MK (parameters from NGC 5548, cf. Kaastra and Barr (1989)). The system is placed at a redshift of 0.033 (i.e. distance 198 Mpc). Due to the redshift several absorption edges (e.g. from O I) due to absorption in our galaxy (column density $N_H = 2\ 10^{20}$ cm^{-2}) and at the source ($N_H = 10^{21}$ cm^{-2}) can be resolved, as well as many thermal emission lines. At long wavelengths the modified blackbody component dominates, at shorter wavelengths the power law. The *redshifted* O VIII line at 19.6 Å can be detected within 10^4 s at the 5σ level for AGN's with a spectrum as shown in Figure 9.

2.2. Nebula-type photoionized plasmas

The nebular model is applicable to an important class of cosmic X-ray sources involving photoionized nebulae. Examples include accretion-powered sources like X-ray binaries, cataclysmic variables, and active galactic nuclei, where a central X-ray emitting region is surrounded by a cooler, partially ionized medium. Other examples are early-type stars in which X-rays produced in a hot corona must be transferred outward through a stellar wind, and stellar sources located near the nucleus of normal galaxies which are surrounded by the local interstellar medium.

In all these cases photoelectric absorption edges will substantially modify the emergent X-ray spectrum particularly at

longer wavelengths. High-resolution spectral measurements of the strength of K-shell absorption edges in combination with emission lines produced by recombination, provide information on the geometry of the medium surrounding the source along the line of sight. The nebular model (e.g. Holt and McCray 1982, McCray 1982, 1984, Kallman and McCray 1982) is the X-ray analogue of a planetary nebula, in which a central continuum source ionizes the surrounding gas. The gas may be optically thick to photoabsorption but not to electron scattering. The ionization and temperature structure of the gas are established by a stationary balance between photoionization (collisional ionization can be neglected) and heating due to the central X-ray source and, on the other hand, (radiative plus dielectronic) recombination and charge exchange and cooling of the gas. When the gas is optically thin, the local radiation field is determined by geometrical dilution of the source spectrum. Then the local state of the gas (at radius R from the central X-ray source) can be parametrized in terms of the scaling parameter $\xi = L/nR^2$ (L is the total luminosity of the central source, n is the local gas density).

The model can be applied to a wide variety of astrophysical X-ray sources and ranges from optically thin to optically thick in the photoionization continuum of abundant elements. In the latter case, the transfer of continuum radiation should be taken into account.

It may be instructive to contrast the nebular model with the coronal model. In the latter model the mechanism for heating the gas is not specified, but the heat input is coupled directly to the ions and free electrons. The parameters characterizing this model are electron temperature, element abundances, and emission measure. At a given temperature only one or two ionization stages of a given element are abundant. In the nebular model the temperature of the gas is not a free parameter, but instead is determined by absorption and emission of radiation in the gas. The elements are primarily ionized by innershell photoionization. As a result a wider range of ionization stages of a given element can simultaneously occur

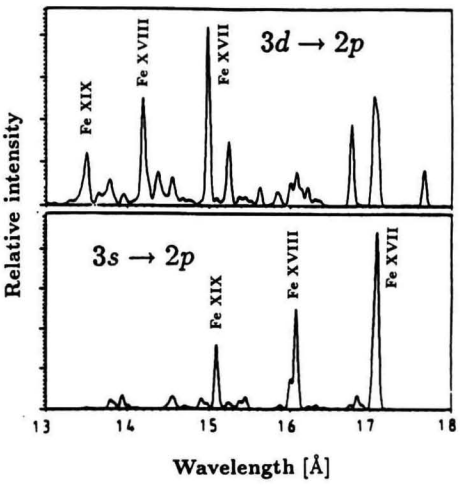

Fig. 10. Model spectra of Fe XVII–XIX from 13–18 Å with 0.052 Å resolution calculated by Liedahl *et al.* (1989). Both spectra are plotted on the same scale, wavelength in Å, intensity in arbitrary units. *Top:* Collisional equilibrium with T = 5.75 MK for the electron temperature. The strong lines at 13.5, 14.2, and 15.0 Å (from Fe XIX, XVIII, and XVII, respectively) are collisionally excited 3*d* lines. *Bottom:* Recombination-dominated spectrum at T=0.11 MK and ionization structure appropriate to an X-ray photoionized nebula. The prominent lines at 15, 16, and 17 Å (from Fe XIX, XVIII, and XVII) are all recombination-cascade-populated 3*s* lines, which cannot be excited by electron collisions at this low electron temperature. The electron density is in each case 10^{11} cm^{-3}.

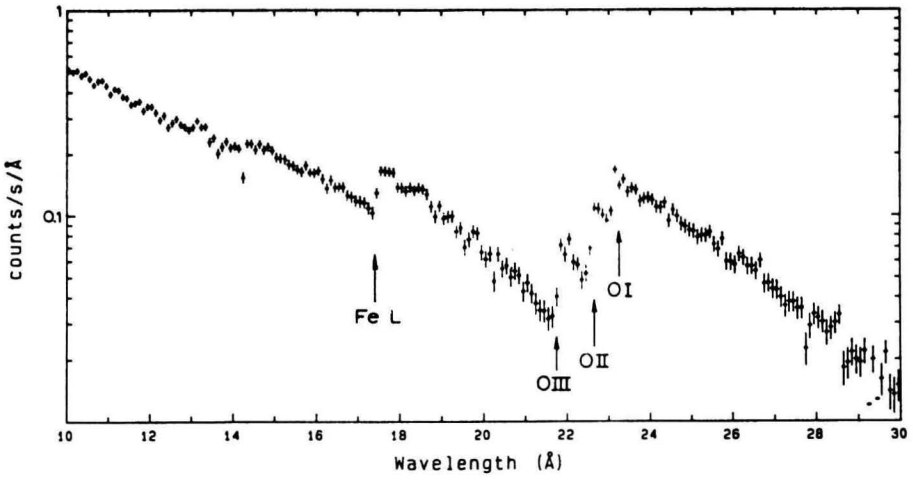

Fig. 11. Simulated *AXAF–LETGS* spectrum of a strong compact X-ray source, observed for 10^4 s with a resolution of 0.1 Å. Interstellar hydrogen column density $N_H = 3\ 10^{21}$ cm^{-2}.

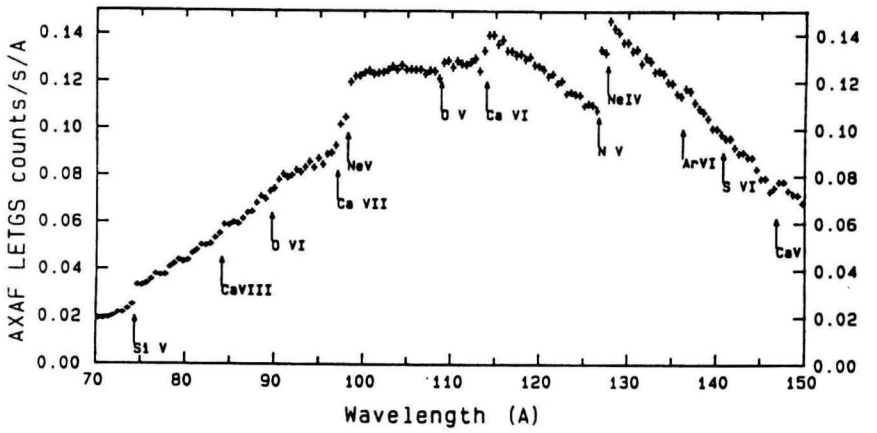

Fig. 12. A hot DA white dwarf (effective temperature 0.065 MK, magnitude V=15) observation simulation for the *AXAF-LETGS* with an integration time of 10^5 s. Traces of metal abundances are assumed a factor of $\sim$ 10 below the observed abundances in the DA dwarf Feige 24 and slightly above the upper limits observed in the hot DA dwarf HZ 43 (Paerels *et al.* 1986). Interstellar column density $N_H = 3\ 10^{19}$ cm^{-2}.

and the elements are more highly ionized ("overionized") at a given temperature than they would be in the coronal model. The emergent X-ray spectrum consists of the central continuum with a low-energy cutoff due to photoabsorption and emission lines due to recombination and fluorescence (in the latter case e.g. K-shell lines from ions with nearly stripped L-shells with reasonable radiative yields such as Li-, Be- and B-like ions (Chen 1986, Chen and Crasemann 1987)) in the nebula, typically near the continuum absorption cutoff.

X-ray photoionized plasmas can differ from collisionally ionized plasmas with similar ion concentrations. Because the photoionized plasma is *overionized* relative to the electron temperature, the excitations of important lines are dominated by recombination, photoexcitation, and cascades as opposed to collisional excitation and dielectronic recombination. This has a drastic effect on the emergent spectrum, as illustrated in Figure 10, where I have plotted spectra calculated for Fe XVII - XIX ions assuming coronal and photoionized conditions respectively (Liedahl *et al.* 1989). As can be seen, it will be straightforward to distinguish photoionized plasmas from coronal plasmas with such spectra. The relative line intensities detected in the photoionized case can be shown to be sensitive functions of the density and geometry of the emission regions and of the spectral shape of the photoionizing continuum.

Another means to distinguish the two types of plasma models is density diagnostics (see Figure 4). Deviations from coronal equilibrium can alter this diagnostics through different recombination and ionization effects, but the line intensity ratios remain density-sensitive also for these cases (Pradhan 1985). The *f/i* ratio does not depend on the model because its density dependence is determined only by the collisional coupling between the upper levels of the two lines, but the ratio *(f+i)/r* does. E.g., for the O VII triplet it is $\sim$ 1 in the coronal model (where the lines are excited by electron collisions from the ground) and $\sim$ 3 in the photoionized nebular model (where population occurs through recombination, directly or via cascades). Hence this diagnostic tool can be quite generally applied to many astrophysical and laboratory sources, while the singlet/triplet ratio can be used as an indication of the model conditions.

2.3. *Optically thick plasmas*

In the extreme case of very dense plasmas, e.g. those present in the inner regions of accretion flows on compact objects such as very hot white dwarfs (in cataclysmic variables) and neutron stars (in hard X-ray binaries) and in the centre of AGN, the source is optically thick to both continuum and line radiation. The spectrum will resemble, at very high optical depths, blackbody emission or a superposition of blackbody type spectra (cf. also Figure 9). However, at intermediate optical depths, the spectral formation is influenced by complicated radiation transfer effects as well as by fundamental atomic processes. Discrete spectral structure is expected which can provide much information about the source (Ross 1979). For X-ray emitting plasmas, Compton scattering plays a significant role as well where transfer through the scattering plasma will broaden and shift line profiles (in addition to thermal broadening) and alter the continuum distribution, depending on temperature and column density (Lightman *et al.* 1981). The spectral resolving power of the future spectrometers is sufficient to resolve the X-ray spectral features that are indicative of the nature of the Compton scattering processes as well as of the structure of the accretion disk corona or the magnetosphere of the neutron star. Emission features observed from X-ray binaries lie in the wavelength region 9–20 Å and are probably from L-transitions from partially ionized iron atoms (e.g. Vrtilek *et al.* 1986).

The spectrum not only contains information on the primary X-ray source itself, but will be modified by fluorescent emission lines and absorption edges produced by the cooler, surrounding medium. The depth of an absorption edge is a measure of the element responsible for this edge and since the

energy of an edge moves towards higher values with increasing ionization, in this way the population of various ionization stages of the constituents of the circumstellar material can be measured. With high spectral resolution one is able to determine the element abundances of the interstellar medium towards many strong galactic and extragalactic X-ray sources. Figure 11 shows a simulation of the X-ray spectrum of a strong accreting compact X-ray source (integrated X-ray flux at Earth $\sim 3\ 10^{-9}$erg cm^{-2}s^{-1}) with a column density of intervening matter of N_H=3 10^{21}cm^{-2}, observed with the *AXAF–LETGS*. The spectrum shows the possible identification of various ionization stages of oxygen.

Finally, another important class of objects to be studied at very soft X-rays are *isolated* hot white dwarfs with optically thick (in visible and UV) photospheric plasmas with effective temperatures in the range $\sim$ 0.03–0.2 MK. At high gravity all hydrogen is pressure-ionized and the outer layers of the photosphere are transparent to the soft X-ray radiation of hotter and deeper layers which become optically thick to the X-rays. The shape of the X-ray spectra is very sensitive to photospheric parameters like effective temperature, gravity and element abundances (for a review e.g. Heise 1988). Trace amounts of highly ionized metals may produce a variety of absorption edges that can be detected in high-resolution X-ray spectra at long wavelengths and which allows one to accurately determine effective temperatures and element abundances for objects as hot DA and very hot DO white dwarf stars. Figure 12 shows a simulation for an observation of a hot DA white dwarf with very low metal abundances ($\sim 10^{-7}$) at a distance $\sim$ 100 pc (magnitude $V = 15$).

3. SUMMARY

High-resolution X-ray spectroscopy has applications to a wide range of hot astrophysical plasmas. Its significance as a tool in understanding the physics of such sources will depend much on the reliability of theoretical models to interpret the spectra. In this paper I have considered various models used in describing the characteristics of hot plasmas and discussed several examples of the emergent X-ray spectrum to illustrate some of the problems of interpretation. It is clear that the complexity of plasma physics and the atomic parameters involved are such that a sound verification of plasma theories and atomic physics which are applied will be required and that for instance better model calculations with improved collisional excitation and ionization rates for the complex ions will be needed for the interpretation of future *AXAF* and *XMM* X-ray spectra.

ACKNOWLEDGEMENTS

This work has been supported by the Space Research Organization of the Netherlands (SRON).

REFERENCES

Aggarwal, K., Berrington, K., Eissner, W., Kingston, A.: 1986, *"Report on Recommended Data"*, Atomic Data Workshop, Daresbury Lab.

Arnaud, M., Rothenflug, R.: 1985, *Astron. Astrophys. Suppl. Ser.* **60**, 425

Barr, P., *et al.*: 1988, *The High-Throughput X-Ray Spectroscopy Mission: The Mission Science Report*, ESA SP-1097

Brinkman, A.C. *et al.*: 1987, *Astro. Lett. and Communications* **26**, 73

Canizares, C.R. *et al.*: 1987, *Astro. Lett. and Communications* **26**, 87

Chen, M.H.: 1986, *Atom. Data Nuc. Data Tab.* **34**, 301

Chen, M.H., Crasemann, B.: 1987, *Phys. Rev. A* **35**, 4579

Dolder, K., Peart, B.: 1986, *Adv. At. Mol. Phys.* **22**, 197

Dunn, H.: 1986, in *At. Proc. in Electron-Ion and Ion-Ion Collisions*, (ed. F. Brouillard), Plenum Publ. Co., p. 93; in *Electronic and At. Collisions* (ed. D.C. Lorents, W.E. Meyerhof, J.R. Peterson), Elsevier Sc. Publ., p. 23

Elwert, G.: 1952, *Z. Naturf.* **7a**, 432

Gabriel, A.H., Jordan, C.: 1979, *MNRAS* **145**, 241

Gallagher, J.H., Pradhan, A.K.: 1985, JILA Data Center Report No. 30, JILA, Univ. of Colorado, Boulder

Griem, H.R.: 1988, *J. Quant. Spectr. Rad. Transf.* **40**, 403

Hahn, Y.: 1985, *Adv. At. Mol. Phys.* **21**, 123

Heise J.: 1988, in *X-ray Astronomy with EXOSAT* (eds. R. Pallavicini, N.E. White), Memorie della Società Astronomica Italiana **59**, p. 53

Holt, S., McCray, R.: 1982, *Ann. Rev. Astron. Astrophys.* **20**, 323

Kaastra, J.S., Barr, P.: 1989, submitted to *Astron. Astrophys.*

Kaastra, J.S., Mewe, R., Brinkman, A.C.: 1989, to be published

Kallman, T.R., McCray, R.: 1982, *Astrophys. J. Suppl.* **50**, 263

Kingston, A.E., Tayal, S.S.: 1983, *J. Phys. B.* **16**, 3465

Lea, S., Mushotzky, R., Holt, S.S.: 1982, *Astrophys. J.* **262**, 24

Lemen, J.R., Mewe, R., Schrijver, C.J., Fludra, A.: 1989, *Astrophys. J.* **341**, 474

Liedahl, D.A., Kahn, S.M., Osterheld, A.L., Goldstein, W.H.: 1989, in preparation.

Lightman, A.P., Lamb, D.Q., Rybicki, G.B.: 1981, *Astrophys. J.* **248**, 738

Mason *et al.*: 1984, *Solar Phys.* **92**, 199

McCray, R.: 1982, in *Galactic X-ray Sources* (ed. P. Sanford, Wiley & Sons, Chicester), p. 71

McCray, R.: 1984, *Physica Scripta* **T7**, 73

Mewe, R.: 1972, *Astron. Astrophys.* **20**, 215

Mewe, R.: 1984, *Physica Scripta* **T7**, 5

Mewe, R.: 1988, in *Astrophysical and Laboratory Spectroscopy* (eds. R. Brown, J. Lang), Scottish Univ. Summer School in Phys. Publ., p. 129

Mewe, R.: 1989, in *Physical Processes in Hot Cosmic Plasmas* (ed. W. Brinkmann), Kluwer Acad. Publ., in press

Mewe, R. *et al.*: 1982, *Astrophys. J.* **260**, 233

Mewe, R., Gronenschild, E.H.B.M., van den Oord, G.H.J.: 1985, *Astron. Astrophys. Suppl. Ser.* **62**, 197

Mewe, R., Lemen, J.R., van den Oord, G.H.J.: 1986, *Astron. Astrophys. Suppl. Ser.* **65**, 511

Mewe, R., Schrijver, J.: 1978, *Astron. Astrophys.* **65**, 99

Müller *et al.*: 1987, *Phys. Rev. A* **36**, 599

Paerels, F.B.S. *et al.*: 1986, *Astrophys. J.* **308**, 190; **309**, L33

Petre, R., Mushotzky, R.F., Krolik, J.H., Holt, S.S.: 1984, *Astrophys. J.* **280**, 499
Pradhan, A.K.: 1982, *Astrophys. J.* **263**, 477
Pradhan, A.K.: 1985, *Astrophys. J.* **288**, 824
Pradhan, A.K., Shull, J.M.: 1981, *Astrophys. J.* **249**, 821
Raymond, J.C.: 1988, in *Hot Thin Plasmas in Astrophysics* (ed. R. Pallavicini), Kluwer Acad. Publ., Dordrecht, p. 3
Raymond, J.C.: 1989, in *High Resolution X-ray Spectroscopy of Cosmic Plasmas* (eds. P. Gorenstein, M.V. Zombeck), Proc. IAU Coll. 115, Cambridge, U.S.A., Reidel Publ. Co.
Raymond, J.C., Smith, B.W.: 1977, *Astrophys. J. Suppl.* **35**, 419
Ross, R.R.: 1979, *Astrophys. J.* **233**, 334
Schrijver, C.J.: 1985, *Space Sci. Rev.* **40**, 3
Schrijver, C.J., Lemen, J.R., Mewe, R.: 1989, *Astrophys. J.* **341**, 484
Seaton, M.J.: 1975, *Adv. At. Mol. Phys.* **11**, 83
Sylwester, J., Schrijver, J., Mewe, R.: 1980, *Solar Phys.* **67**, 285
Swank, J.H., White, N.E., Holt, S.S., Becker, R.H.: 1981, *Astrophys. J.* **246**, 208
Vrtilek, S.D. *et al.*: 1986, *Astrophys. J.* **307**, 698; **308**, 644
Weisskopf, M.C.: 1987, *Astro. Lett. and Communications* **26**, 1; see also other articles in this volume
Withbroe, G.L.: 1975, *Solar Phys.* **45**, 301

AUTHOR'S ADDRESS

SRON-Laboratory for Space Research, Utrecht
Beneluxlaan 21
3527 HS Utrecht, The Netherlands